Thioglucose functionalized gold nanoparticles as active substrates for surface enhanced Raman spectroscopy of lectins

Cristina Gellini, Alessandro Feis

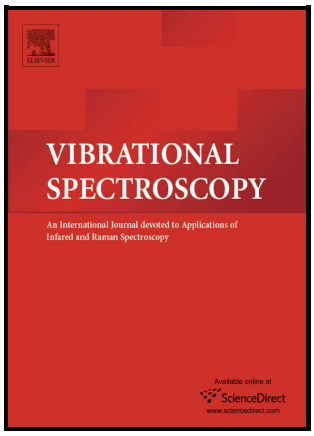

PII: S0924-2031(22)00135-7

DOI: https://doi.org/10.1016/j.vibspec.2022.103468

Reference: VIBSPE103468

To appear in: *Vibrational Spectroscopy*

Received date: 5 August 2022
Revised date: 2 November 2022
Accepted date: 11 November 2022

Please cite this article as: Cristina Gellini and Alessandro Feis, Thioglucose functionalized gold nanoparticles as active substrates for surface enhanced Raman spectroscopy of lectins, *Vibrational Spectroscopy,* (2022) doi:https://doi.org/10.1016/j.vibspec.2022.103468

Thioglucose functionalized gold nanoparticles as active substrates for surface enhanced Raman spectroscopy of lectins

*Cristina Gellini and Alessandro Feis**

Dipartimento di Chimica "Ugo Schiff", Università degli Studi di Firenze, Via della Lastruccia 3, I-50019 Sesto Fiorentino (FI), Italy

ABSTRACT: Vibrational spectroscopy methods display great potential in the study of biomolecules. The complexity of these molecular systems, though, is often a hindrance for the interpretation of the experimental spectra. Selective techniques should therefore be improved and applied extensively. This article presents surface enhanced Raman spectra of an important model protein, namely, wheat germ agglutinin. To obtain these spectra, a novel substrate for the protein has been developed. The substrate is based on gold nanospheroids, produced by wet synthesis. The nanoparticles are then functionalized by reaction with a solution of β-D-thioglucose to increase the affinity of the agglutinin for the surface. When nanoparticle films are placed in contact with diluted agglutinin solutions, vibrational bands of the protein appear and can be easily discriminated from those of the substrate. The Raman bands of the substrate and of the

protein have then been assigned correlatively. On this basis, we conclude that the interaction between the agglutinin and the nanoparticles is selectively detected only when the metal surface is suitably functionalized.

Graphical abstract

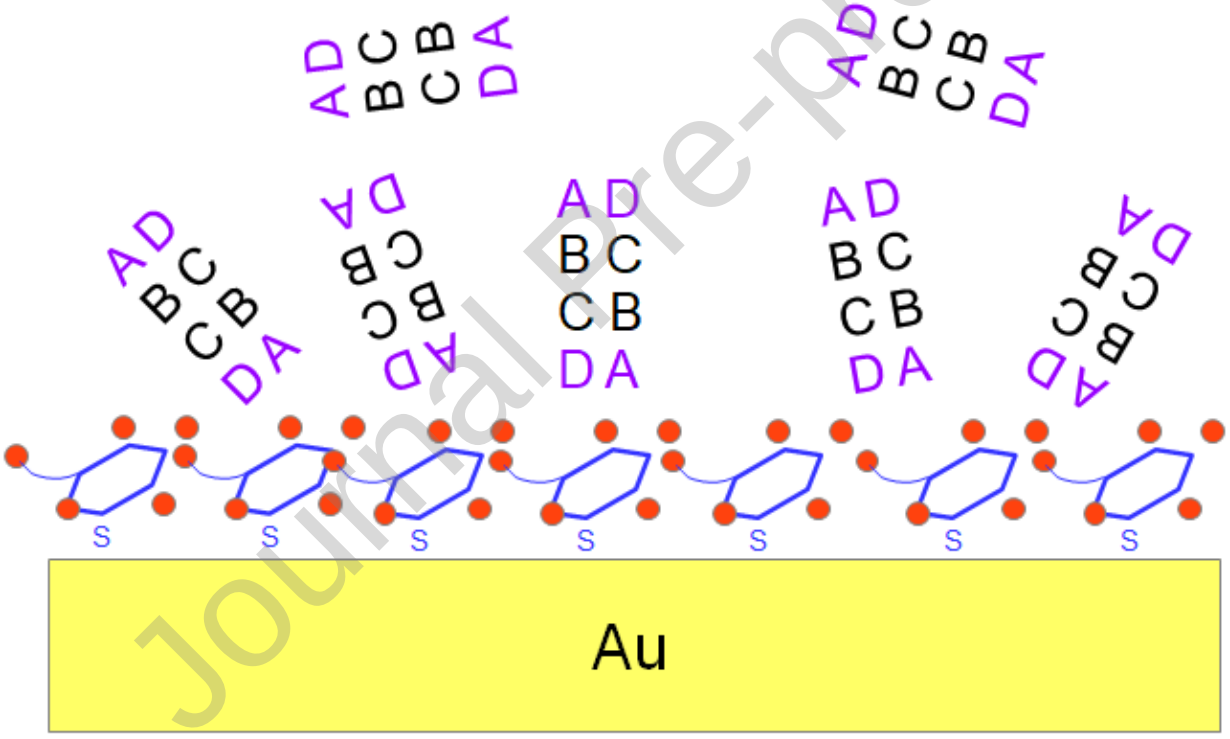

KEYWORDS: Proteins; surface enhanced Raman spectroscopy; functionalized nanoparticles; lectins; sugar recognition.

ABBREVIATIONS: SERS, surface enhanced Raman scattering; WGA, wheat germ agglutinin; AuNPc, gold nanoparticles capped with citrate; AuNPtg, gold nanoparticles functionalized with β-D-thioglucose; Tyr, tyrosine; Trp, tryptophan; Phe, phenylalanine; LSPR, localized surface plasmon resonance.

1. Introduction

Novel physical methods are needed to investigate emerging biomolecule classes. Among these molecules, lectins constitute a large group of carbohydrate-binding proteins. These macromolecules display an especially high importance from both the biological [1-3] and the technological point of view [4]. Lectins are widespread in nature: they can be isolated from viruses, fungi, plants and animals [5,6]. In addition, specifically engineered lectins have been recently developed [7]. The interactions between various lectin types on one side, and glycans or glycoproteins on the other one, represent the molecular basis of many biological events where signaling is involved [8,9]. Molecular specificity towards different carbohydrates is related to the tertiary and quaternary structural properties of each member of this protein family. For instance, galectins can specifically bind galactose, whereas concanavalins display a high affinity for N-acetylglucosamine [1]. Understanding the interactions that are involved in these recognition processes represents an ambitious task in the field of biomolecules. At the molecular level, different roles have been suggested for hydrogen bonding, electrostatic forces, and hydrophobic interactions [10]. This signifies the importance of the presence of aromatic amino acid residues in the sugar binding sites of lectins [11].

Several physicochemical methods are currently applied to the study of lectins. X-ray crystallography, in particular, has yielded a large number of structures of these proteins, alone or complexed with various kinds of saccharides as oligomers or polymers [12]. Magnetic resonance spectroscopy methods are also exploited to obtain valuable information about the intermolecular interactions between lectins and sugars in aqueous media [13,14]. Thermodynamics of the complexation process is widely characterized by calorimetric methods [15]. Optical techniques, on the other hand, have a high information potential. They can yield details about the intermolecular interactions giving rise to lectin / sugar complexes and can be performed at relatively low concentrations. Vibrational spectroscopy, when carefully applied, can contribute to very promising methods. These methods, though, are often hindered by the extremely high number of vibrational degrees of freedom, belonging both to proteins and to saccharides, making infrared and Raman studies difficult on the experimental and interpretative side. Therefore, vibrational spectroscopic methods can be aided by variants offering the advantage of selectivity. Resonance Raman spectroscopy and surface enhanced Raman scattering (SERS) spectroscopy are representative examples of the improvement given by selectivity to spectroscopic studies, especially in the field of biologically active molecules [16-19].

SERS spectra of biomolecules are often difficult to be measured, as a SERS-active substrate is required to ensure substantial enhancement of the Raman signals [20]. Not all nanostructured materials are suitable for this task. Metal nanoparticles are most commonly employed because of their favorable optical properties [21-23]. On the other hand, their surface may give rise to a chemical reaction with the adsorbed molecules. In this event the resulting SERS spectra will be changed and produce misleading information [24]. This issue explains the need for a protection of the surface, often translated into a functionalizing coating [25-27]. An ideal coating should

avoid chemical reactions with the metal, while keeping the adsorbed molecules at a short distance from the surface. Moreover, the functionalization agent should impart selective affinity for the (macro)molecule studied by SERS. In the field of biomolecule research, much experimental work has been performed with functionalized nanoparticles either as colloidal dispersions, or cast as solid substrates that are placed in contact with biomolecule solutions [28,29].

In the present study we have applied SERS spectroscopy to obtain Raman spectra of a model lectin. We have chosen wheat germ agglutinin (WGA) as a model, as this protein is widely known from the structural and physicochemical point of view [30,31]. The goal is the measurement of protein Raman spectra in diluted aqueous solution, taking advantage of the signal enhancement by metal nanoparticles. It is widely recognized that bringing macromolecules close to the metal nanoparticle surface, that is the first step in generating SERS spectra, is not straightforward. This task can be made easier by chemical modifications at the surface, i.e., by functionalization. In the case of lectins, saccharides appear to be the first choice in an attempt to promote the interaction between metal nanoparticles and proteins [32-35]. Therefore, we have first produced gold nanoparticles by a well-characterized reaction, and we have successively functionalized the metal surface by a reaction with β-D-thioglucose. We have finally employed the product of this reaction as a substrate to perform SERS spectroscopy of WGA.

2. Materials and methods

$HAuCl_4$ (99.999 % purity), sodium citrate (99.5 % purity) and WGA (100 % purity) were purchased by Sigma. β-D-thioglucose (97% purity) was purchased by Alfa Aesar. H_2O (Lichrosolv grade) was purchased by Merck. Au dispersions were synthesized by citrate reduction according to Frens' procedure [36], that is based on previous work by Turkevich [37, 38]. Aqueous solutions of β-D-thioglucose were employed for the functionalization [39]. The solutions were mixed with the Au dispersions at room temperature, reaching the final β-D-thioglucose concentration 4×10^{-6} M or 5×10^{-7} M.

The substrates for SERS spectroscopy were obtained from concentrated nanoparticle dispersions. The dispersions were centrifuged at 3000 rpm for 10 minutes at 20°C to increase the nanoparticle concentration by a factor 12. This factor was estimated by measurements of the dispersion volume before and after centrifugation. The volumes were measured by calibrated Nichiryo pipettes. A drop of the concentrated dispersion was deposited on a microscope cover glass and dried for 30 minutes at room temperature until a film was formed. Representative micrographs of the film samples are shown in Figure SM 1 of the Supplementary Material section. The glass was successively put on the well of a microscope slide, containing either the protein solution or pure water for reference measurements.

UV-visible extinction spectra were measured with an Agilent Cary5 spectrophotometer. The optical path was 1 cm.

SERS spectra were measured with a Renishaw RM 2000 microRaman spectrometer. An objective 60× was employed. The laser excitation wavelength was 785 nm. The power at the sample, measured with a Coherent Field Master detector equipped with an LM-2 head, was 170 μW. The signal integration time was 10 s for each spectral acquisition. A variable number of

spectra were averaged, depending on the signal-to-noise ratio that could be obtained by each sample.

Ordinary Raman spectra were measured with a Bruker MultiRam spectrometer on pure solid samples. The laser excitation wavelength was 1064 nm. The spectral resolution was 4 cm^{-1}.

3. Results

We first describe a comparative optical study on aqueous dispersions of citrate-reduced Au nanospheres (AuNPc) and β-D-thioglucose functionalized Au nanospheres (AuNPtg) without protein. The localized surface plasmon resonance (LSPR) band displays an extinction maximum at 531 nm for AuNPc dispersions. The layer of functionalizing β-D-thioglucose molecules determines a slight shift of the LSPR maximum of AuNPtg to 533 nm. This shift can be related to the dielectric constant increase due to the replacement of citrate molecules by β-D-thioglucose in the substitution reaction.

Figure 1 a displays the SERS spectrum of an AuNPc film in contact with pure water. The most intense band in the examined wavenumber range is observed at 247 cm^{-1}. Several other medium-intensity SERS bands are present in the range 900-1600 cm^{-1}. The wavenumbers are reported in Table 1, together with a correlative assignment.

(Figure 1)

Figure 1. (a) SERS spectrum of an AuNPc film. (b) SERS spectrum of a film of AuNPtg functionalized by a 4×10^{-6} M β-D-thioglucose solution. The films are in contact with pure water during the SERS measurement.

Figure 1 b shows the SERS spectrum of an AuNPtg film sample functionalized by a 4×10^{-6} M β-D-thioglucose solution. The spectra are measured in similar experimental conditions as those of AuNPc. Strong variations can mainly be observed in the low-frequency range. In particular, two bands appear at 261 cm^{-1} and at 295 cm^{-1}. The wavenumber range 500-1300 cm^{-1} shows additional medium-intensity bands, suggesting they are related to β-D-thioglucose binding to the Au surface. To verify this explanation, we have measured SERS spectra of films obtained by functionalization at intermediate β-D-thioglucose concentration. An example of these spectra is shown in Figure SM 2 of the Supplementary Material part.

To gain insight into the vibrational features of β-D-thioglucose, we have performed a Raman spectrum of pure β-D-thioglucose in the solid state, displayed in Figure 2 in the region between 200 and 1800 cm^{-1}. Seventeen bands are shared by both the Raman spectrum of the solid sample and the SERS spectrum shown in Figure 1 b. Direct comparison of β-D-thioglucose Raman and SERS spectra can be found as supplementary information (Figure SM 2 of the Supplementary Material part). The wavenumbers of solid β-D-thioglucose bands are listed in Table 1, together with the vibrational assignments proposed in previous SERS investigations about β-D-thioglucose on various metal surfaces [40,41].

(Figure 2)

Figure 2. Raman spectrum of pure solid β-D-thioglucose. The laser power at the sample is 60 mW. 3000 interferograms are averaged.

Table 1. Experimental wavenumbers observed in the Raman spectrum of solid β-D-thioglucose, in the SERS spectra of AuNPtg films, and in the SERS spectra of AuNPc films. Abbreviations: ν, stretching; ν_s, symmetric stretching; ν_{as}, asymmetric stretching; δ, bending; τ, torsion; ρ, rocking; ω, wagging.

AuNPc SERS (Figure 1 a)	AuNPtg SERS (Figure 1 b)	Solid β-D-thioglucose Raman (Figure 2)	Assignment
247			ν (Au-O) [42]
	261		Radial Au-S displacements [43]
	295		Tangential Au-S displacements [43]
		356	δ(CCC) [41]
		415	τ(OH) [41]
		435	δ(CCC) [41]
		513	δ(CCO) [41]
	532	550	τ(CCO) [41]
	718	710	τ(CCC) [41]

802			ν (C-O), ρ(CH_2) [44]
	~ 820	819	ν (CS) [40]
	~ 880	897	ν (CC) / ν_s (COC) ring / ρ(CH_2) [40,41]
	922	913	ν (CC) / ν_s (COC) ring / ρ(CH_2) [40,41]
	997	993	ν (CO) [41]
1030			ν (C-C-O) [44]
	1026	1031	ν (CC) ring / ν (COC) ring / δ(COH) [40]
	1053	1048	ν (CC) ring / ν (COC) ring / δ(COH) [40]
			ν (C-OH) [41]
		1064	ν (CC) ring / δ(COH) [40]
		1084	ν (CC) ring / ν (COC) ring / δ(COH) [40,41]
	1115	1112	ν (C-OH) [41]
		1136	ν (COC) ring / ν (C-OH) [40]
	1175	1195	ω(CH), δ(CH) [40,41]
	1215	1226	δ (COH, CH) [40,41]
1255			ν (C-O)
	1259	1270	τ(CH_2) [41]
1300			ν (C-O)[44]
	1298	1328	ω(CH_2), τ(OH) [41]
1348			ν_s (COO^-) [45]
	1358	1356	δ (COH, CH) [40]
1376			ν_s (COO^-) [45]
	1378	1376	δ (COH, CH) [40] , ω(CH_2), τ(OH) [41]
		1408	ν(CCC) [41]
1430			(CH_2) deformation
	1435	1459	ω (CH_2) / δ (CH_2, COH, CH) [40]

1536 $\nu_{as}(COO^{-})$

The effect of the functionalization of the Au nanoparticles can be highlighted by a comparison between the extinction spectra of AuNPc dispersions and those of AuNPtg dispersions when WGA at increasing concentration is added (Figure 3). In the case of AuNPc, the presence of a very small amount of WGA (1×10^{-9} M) clearly gives rise to a red shifted, broad LSPR band due to nanoparticle aggregation. Further increases of the protein concentration shift the extinction maximum to 717 nm. The AuNPtg dispersions show a different behavior. The extinction spectrum of AuNPtg is not altered by WGA additions below 7×10^{-8} M. When the protein concentration is further increased, the LSPR band of aggregated nanoparticles only shifts to 634 nm.

(Figure 3)

Figure 3. (a) Extinction spectra of AuNPc dispersed in water at increasing WGA concentration. (b) Extinction spectra of AuNPtg dispersed in water at increasing WGA concentration.

When films of AuNPtg and AuNPc are formed, it can be observed that the interaction with WGA gives rise to different SERS spectra for the two samples (Figure 4). In fact, protein SERS bands are observed when the films consist of functionalized AuNPtg nanoparticles. The protein

bands, detected at a very low (5×10^{-6} M) WGA concentration, are overlapped with those of β-D-thioglucose. For a better comparison, we contrast the SERS spectrum of WGA in solution with the solid protein Raman spectrum in the 400-1100 cm^{-1} region in Figure 5. The SERS bands at 646, 718, 760, and 1012 cm^{-1} can be interpreted as vibrational bands of the amino acid side chains, as it will be explained in the Discussion section. An extended Raman spectrum of solid WGA is reported in Figure SM 3 of the Supplementary Material part. To assign the Raman bands of WGA we have extensively searched for correlations with literature data (Table 2).

(Figure 4)

Figure 4. (a) SERS spectrum of an AuNPc film placed in contact with a 5×10^{-6} M WGA solution. (b) SERS spectrum of an AuNPtg film functionalized with a 4×10^{-6} M β-D-thioglucose solution, successively placed in contact with a 5×10^{-6} M WGA solution.

(Figure 5)

Figure 5. The SERS spectrum of 5×10^{-6} M WGA solution in Figure 4 b (upper trace) is compared with the Raman spectrum of solid WGA (lower trace) in the wavenumber region 400-1100 cm^{-1}. The Raman spectrum of solid WGA in the 200-1800 cm^{-1} range is reported in Figure SM 3.

Table 2. Experimental wavenumbers observed for solid WGA and for WGA adsorbed on AuNPtg films. Band assignments from literature are proposed.

Solid WGA Raman	WGA SERS on AuNPtg	Assignment
	261, 293	β-D-thioglucose Au-S displacements [43]
307		
421		Tyr [46]
509		S-S stretching [47-49]
622		Phe [46]
645	646	Cys [50] Tyr [46, 51, 52]
658		Met [50]
675		Cys [48]
722	718	Met [51]
761	760	Trp [51-54]
782		Cys [48]
806		Tyr [51]
836		Tyr [51-53]
856		Tyr [51-53]

881		Trp [51, 53]
937		Skeletal deformation [51]
966		Trp [51]
988		Arg [55]
1005		Phe [46, 51, 53]
1013	1012	Trp [52, 53]
1032		Phe [46, 51, 53]
1076	1072	Arg [55]
1124		C-N [51]
1183		Tyr [51, 56]
1209		Tyr, Phe [51, 56]
1236		Amide III [57]
1254		Amide III [57]
1307		Cys [50]
1338	1340	Trp [51-53, 58]
1361		Trp [52, 58]
1415		δ(C-H) [51]
1445		δ(C-H) [51]
1552		Trp [51, 53]
1585		Tyr [56]
1606		Phe, Tyr [56]
1615		Tyr [56]
1651		Amide I [58]
1673		Amide I [59]

4. Discussion

The significance of the nanoparticle functionalization by β-D-thioglucose can be evaluated by contrasting the extinction spectra of AuNPc and AuNPtg that are shown in Figure 3. The behavior of the AuNPc and AuNPtg dispersions is strongly different when WGA is added to the nanoparticles. The unfunctionalized AuNPc samples are aggregated in the presence of minimal WGA concentrations, with a LSPR shift to 717 nm. The large shift of the LSPR maximum points to an extensive aggregation, possibly involving several Au nanoparticles [60,61]. The formation of large aggregates has been reported in other studies, e.g., upon addition of bovine serum albumin to 30 nm Au nanoparticles [62]. When the albumin-induced aggregates contained hundreds of Au nanoparticles, they displayed an LSPR maximum at ~ 720 nm, as it was shown by analytical ultracentrifugation combined with extinction measurements. Interestingly, when the aggregates consisted of Au nanoparticle dimers and trimers, the maximum was in the range 600–650 nm. This observation suggests that the interaction of WGA with AuNPtg, that yields limited shift of the LSPR maximum to 634 nm, similarly is due to the formation of few-nanoparticle aggregates. It is tempting to interpret the different behavior of AuNPtg and AuNPc through intermolecular interactions at the AuNP surface. This means that the surface-bound β-D-thioglucose units bind the protein molecules at their glycan-binding sites with some degree of specificity. The resulting complex could bind one more AuNP – or a few more nanoparticles. Further growth of the aggregate would stop at this stage in AuNPtg. At variance, the

agglomeration of AuNPc would occur in a chaotic process where several nanoparticles are juxtaposed in various orientations involving multiple kinds of protein / AuNPs interactions.

The different way of complex formation can explain the main result of the present study, namely, protein SERS bands appearing upon WGA adsorption on AuNPtg. This result is in stark contrast with the minimal effect induced by WGA on the SERS spectra of AuNPc samples. In that case spectral changes are restricted below 300 cm^{-1} (Figure 4 a), where the vibrational bands involving the metal displacements are detected. This observation suggests that the protein and the AuNPc nanoparticles are involved in an interaction, although the SERS bands of the protein moiety are not detected. It is possible that the protein bands are hidden in the broad background because of the structural heterogeneity of the protein / AuNPc complexes, as observed in the UV-visible spectra discussed above. This would correspond to the spectral heterogeneity of SERS as well, leading to broadened bands that are not easily distinguished from the background.

Conversely, many SERS features of the AuNPtg / WGA complexes can be interpreted as characteristic protein bands. It can be foreseen that the protein bands that are most prominent are related to vibrational modes of aromatic amino acids [52]. These residues in each protein monomer are eight tyrosine residues (Tyr) in WGA isolectin 1 (seven in isolectin 2), three tryptophan residues (Trp), and three phenylalanine residues (Phe) [63]. Three bands of Trp [53] are clearly detected in the SERS spectra in Figure 4 b at 760, 1012 and 1340 cm^{-1}. The Trp bands at higher wavenumbers are largely overlapped with β-D-thioglucose bands. In contrast, the contributions of Tyr to the spectrum are detected less easily, possibly because of a larger bandwidth. However, the SERS band at 646 cm^{-1} can be related to Tyr [51,56]. No Phe bands are observed. It is apparent that the intensity of the SERS bands is not proportional to the relative abundance of each aromatic amino acid residue. The intensity enhancement, in fact, is strongly

dependent on the amino acid position in the protein, as this is related to the distance from the metal surface when the protein is adsorbed. A relationship between the SERS enhancement factor and the distance from the nanoparticle surface has been established both theoretically and experimentally for several systems [21]. Besides the bands of the aromatic amino acids, moderately enhanced contributions can be ascribed to other residues, i.e., cysteine (Cys) at 646 cm^{-1} [50] overlapped with a Tyr band, and methionine (Met) at 718 cm^{-1} [51]. The SERS bands in the region within 800 and 950 cm^{-1} (Figure 4 b) are largely broadened. This is possibly a hindrance for the detection of single bands.

The SERS results can be interpreted through one of the three-dimensional models of the glycan binding sites of WGA proposed on the basis of X-ray crystallography and computational results [31]. Four different protein domains have been proposed and termed A, B, C, and D for each monomer. Each domain contains a sugar binding site that includes a serine residue and aromatic amino acids. The A domain binding site presents three Tyr residues in the positions 21, 23, and 30, not far from a Trp residue that occupies position 41. The site in the B domain is structurally similar to that in A, except for the absence of a Trp residue near the binding site. The aromatic residues involved in binding at the C domain are one Trp and two Phe. Finally, the D domain binding site only involves two aromatic residues, i.e., Trp and Tyr. As only Tyr and Trp bands can be detected in the SERS spectra of the protein adsorbed on AuNPtg, it is likely that A and D sites are mainly involved in the interaction between WGA and the thiosaccharide moiety of AuNPtg.

5. Conclusions

Our study shows the importance of a targeted functionalized surface for the detection of protein vibrational features by SERS. In fact, we have contrasted useful results obtained by different spectroscopic methods, namely, electronic absorption and SERS spectroscopy. UV-visible absorption unequivocally shows that WGA / Au nanoparticle interactions occur both for citrate-capped metal surfaces and for β-D-thioglucose coated nanoparticles. However, only the latter substrate can give rise to SERS spectra displaying vibrational bands of the amino acid side chains. We have observed bands that can be assigned to the side chains of Trp, Cys, Arg, Met and Tyr on the basis of a correlation between the experimental Raman spectrum and literature data. In addition, we have found that the occurrence of these SERS bands is consistent with the three-dimensional properties of the sugar-binding sites of WGA previously proposed by crystallographic and computational studies. We propose that the present study opens the way to future investigations that focus on subtle conformational changes of lectins, including functionally significant variations stemming from the interactions between lectins and glycans [64]. This proposal relies on the informative potential that is typical of SERS in the field of protein research. This kind of vibrational spectroscopy can shed light on molecular properties and intermolecular interactions, and permit the detection of macromolecules for analytical purposes.

CRediT authorship contribution statement

Cristina Gellini : conceptualization; methodology; investigation ; writing; visualization; supervision; funding acquisition.

Alessandro Feis : conceptualization; methodology; investigation ; writing; visualization; supervision; funding acquisition.

Declaration of interests

☒ The authors declare that they have no known competing financial interests or personal relationships that could have appeared to influence the work reported in this paper.

☐The authors declare the following financial interests/personal relationships which may be considered as potential competing interests:

References

[1] H. Lis and N. Sharon, Lectins: carbohydrate-specific proteins that mediate cellular recognition, Chem. Rev. 98 (1998) 637−674.

[2] M. Ambrosi, N. R. Cameron and B. G. Davis, Lectins: tools for the molecular understanding of the glycocode, Org. Biomol. Chem. 3 (2005) 1593−1608.

[3] S. Cecioni, A. Imberty and S. Vidal, Glycomimetics versus multivalent glycoconjugates for the design of high affinity lectin ligands, Chem. Rev. 115 (2015) 525−561.

[4] X. Dan, W. Liu and T. B. Ng, Development and applications of lectins as biological tools in biomedical research, Med. Res. Rev. 36 (2016) 221–247.

[5] E. M. Ward, M. E. Kizer and B. Imperiali, Strategies and Tactics for the Development of Selective Glycan-Binding Proteins, ACS Chem. Biol. 16 (2021) 1795−1813.

[6] E. J. M. Van Damme, 35 years in plant lectin research: a journey from basic science to applications in agriculture and medicine, Glycoconjugate J. 39 (2022) 83–97.

[7] J. Hirabayashi and R. Arai, Lectin engineering: the possible and the actual, Interface Focus 9 (2019) 20180068.

[8] K. Drickamer and M. E Taylor, Recent insights into structures and functions of C-type lectins in the immune system, Curr. Opin. Struct. Biol. 34 (2015) 26–34.

[9] Y. Kim, J. Y. Hyun and I. Shin, Multivalent glycans for biological and biomedical applications, Chem. Soc. Rev. 50 (2021) 10567−10593.

[10] L. L. Kiessling and R. C. Diehl, CH−π Interactions in Glycan Recognition, ACS Chem. Biol. 16 (2021) 1884−1893.

[11] K. L. Hudson, G. J. Bartlett, R. C. Diehl, J. Agirre, T. Gallagher, L. L. Kiessling and D. N. Woolfson, Carbohydrate−Aromatic Interactions in Proteins, J. Am. Chem. Soc. 137 (2015) 15152−15160.

[12] R. Loris, T. Hamelryck, J. Bouckaert and L. Wyns, Legume lectin structure, Biochimica et Biophysica Acta 1383 (1998) 9–36.

[13] V. Roldós, F. J. Cañada and J. Jiménez-Barbero, Carbohydrate–protein interactions: a 3d view by NMR, ChemBioChem 12 (2011) 990 – 1005.

[14] R. J. Woods, Predicting the Structures of Glycans, Glycoproteins, and Their Complexes, Chem. Rev. 118 (2018) 8005−8024.

[15] T. K. Dam and C. F. Brewer, Thermodynamic studies of lectin-carbohydrate interactions by isothermal titration calorimetry, Chem. Rev. 102 (2002) 387-429.

[16] S. Schluecker, Surface-enhanced Raman spectroscopy: concepts and chemical applications, Angew. Chem., Int. Ed. 53 (2014) 4756−4795.

[17] L. A. Lane, X. Qian and S. Nie, SERS nanoparticles in medicine: from label-free detection to spectroscopic tagging, Chem. Rev. 115 (2015) 10489−10529.

[18] D. Cialla-May, X. S. Zheng, K. Weber and J. Popp, Recent progress in surface-enhanced Raman spectroscopy for biological and biomedical applications: from cells to clinics, Chem. Soc. Rev. 46 (2017) 3945−3961.

[19] D. Cialla-May, C. Krafft, P. Rösch, T. Deckert-Gaudig, T. Frosch, I. J. Jahn,

S. Pahlow, C. Stiebing, T. Meyer-Zedler, T. Bocklitz, I. Schie, V. Deckert and J. Popp, Raman Spectroscopy and Imaging in Bioanalytics, Anal. Chem. 94 (2022) 86−119.

[20] H. Chen, Z. Cheng, X. Zhou, R. Wang and F. Yu, Emergence of Surface-Enhanced Raman Scattering Probes in Near-Infrared Windows for Biosensing and Bioimaging, Anal. Chem. 94 (2022) 143−164.

[21] E. Le Ru and P. Etchegoin, Principles of Surface-Enhanced Raman Spectroscopy and related plasmonic effects (Elsevier, Amsterdam, Oxford, 2008).

[22] M. Moskovits, Surface-enhanced Raman spectroscopy: a brief retrospective, J. Raman Spectrosc. 36 (2005) 485–496.

[23] S. E. J. Bell, G. Charron, E. Cortés, J. Kneipp, M. Lamy de la Chapelle, J. Langer, M. Procházka, V. Tran and S. Schlücker, Towards Reliable and Quantitative Surface-Enhanced Raman Scattering (SERS): From Key Parameters to Good Analytical Practice, Angew. Chem. Int. Ed. 59 (2020) 5454–5462.

[24] C. Zong, M. Xu, L.-J. Xu, T. Wei, X. Ma, X.-S. Zheng, R. Hu and B. Ren, Surface-enhanced Raman spectroscopy for bioanalysis: reliability and challenges, Chem. Rev. 118 (2018) 4946−4980.

[25] S. Zeng, K.-T. Yong, I. Roy, X.-Q. Dinh, X. Yu and F. Luan, A Review on Functionalized Gold Nanoparticles for Biosensing Applications, Plasmonics 6 (2011) 491–506.

[26] H. Kang, J. T. Buchman, R. S. Rodriguez, H. L. Ring, J. He, K. C. Bantz and C. L. Haynes, Stabilization of Silver and Gold Nanoparticles: Preservation and Improvement of Plasmonic Functionalities, Chem. Rev. 119 (2019) 664−699.

[27] J. W. Lee, S.-R. Choi and J. H. Heo, Simultaneous Stabilization and Functionalization of Gold Nanoparticles via Biomolecule Conjugation: Progress and Perspectives, ACS Appl. Mater. Interfaces 13 (2021), 42311−42328.

[28] I. Bruzas, W. Lum, Z. Gorunmez and L. Sagle, Advances in surface-enhanced Raman spectroscopy (SERS) substrates for lipid and protein characterization: sensing and beyond, Analyst 143 (2018) 3990−4008.

[29] L. Martinez and L. He, Detection of Mycotoxins in Food Using Surface-Enhanced Raman Spectroscopy: A Review, ACS Appl. Bio Mater. 4 (2021) 295−310.

[30] C. Schubert Wright, Crystal structure of a wheat germ agglutinin / glycophorin-sialoglycopeptide receptor complex: structural basis for cooperative lectin-cell binding, J. Biol. Chem. 267 (1992) 14345−14352.

[31] C. Schubert Wright and G. E. Kellogg, Differences in hydropathic properties of ligand binding at four independent sites in wheat germ agglutinin-oligosaccharide crystal complexes, Protein Sci. 5 (1996) 1466−1476.

[32] M. Marradi, F. Chiodo, I. García and S. Penadés, Glyconanoparticles as multifunctional and multimodal carbohydrate systems, Chem. Soc. Rev. 42 (2013) 4728−4745.

[33] X. Li, S. J. H. Martin, Z. S. Chinoy, L. Liu, B. Rittgers, R. A. Dluhy and G.-J. Boons, Label-Free Detection of Glycan–Protein Interactions for Array Development by Surface-Enhanced Raman Spectroscopy (SERS), Chem. Eur. J. 22 (2016) 11180–11185.

[34] F. Compostella, O. Pitirollo, A. Silvestri and L. Polito, Glyco-gold nanoparticles: synthesis and applications, Beilstein J. Org. Chem. 13 (2017) 1008–1021.

[35] L. Guerrini, R. A. Alvarez-Puebla and N. Pazos-Perez, Surface Modifications of Nanoparticles for Stability in Biological Fluids, Materials 11 (2018) 1154.

[36] G. Frens, Controlled nucleation for the regulation of the particle size in monodisperse gold suspensions, Nature Phys. Sci. 241 (1973) 20−22.

[37] J. Turkevich, P.C. Stevenson and J. Hillier, A study of the nucleation and growth processes in the synthesis of colloidal gold, Discuss. Faraday Soc. 11 (1951) 55−75.

[38] B.V. Enüstün and J. Turkevich, Coagulation of colloidal gold, J. Am. Chem. Soc. 85 (1963) 3317−3328.

[39] F. Porcaro, C. Battocchio, A. Antoccia, I. Fratoddi, I. Venditti, A. Fracassi, I. Luisetto, M.V. Russo and G. Polzonetti, Synthesis of functionalized gold nanoparticles capped with 3-mercapto-1-propansulfonate and 1-thioglucose mixed thiols and "in vitro" bioresponse, Colloids and Surfaces B: Biointerfaces 142 (2016) 408–416.

[40] S. R. Smith, R. Seenath, M. R. Kulak and J. Lipkowski, Characterization of a self-assembled monolayer of 1-thio-β-D-glucose with electrochemical surface enhanced Raman spectroscopy using a nanoparticle modified gold electrode, Langmuir 31 (2015) 10076−10086.

[41] M. Vezvaie, C. L. Brosseau, J. D. Goddard and J. Lipkowski, SERS of β-Thioglucose Adsorbed on Nanostructured Silver Electrodes, ChemPhysChem 11 (2010) 1460–1467.

[42] G. L. Beltramo, T. E. Shubina and M. T. M. Koper, Oxidation of Formic Acid and Carbon Monoxide on Gold Electrodes Studied by Surface-Enhanced Raman Spectroscopy and DFT, ChemPhysChem 6 (2005) 2597–2606.

[43] T. Bürgi, Properties of the gold–sulphur interface: from self-assembled monolayers to clusters, Nanoscale 7 (2015) 15553−15567.

[44] V.H. S. deMelo, V. M. Zamarion, K. Araki and H. E. Toma, New insights on surface-enhanced Raman scattering based on controlled aggregation and spectroscopic studies, DFT calculations and symmetry analysis for 3,6-bi-2-pyridyl-1,2,4,5-tetrazine adsorbed onto citrate-stabilized gold nanoparticles, J. Raman Spectrosc. 42 (2011) 644–652.

[45] M. Kerker, O. Siiman, L. A. Bumm and D.-S. Wang, Surface enhanced Raman scattering (SERS) of citrate ion adsorbed on colloidal silver, Appl. Opt. 19 (1980) 3253–3255.

[46] C. Blum, T. Schmid, L. Opilik, S. Weidmann, S. R. Fagerer, R. Zenobi, Understanding tip-enhanced Raman spectra of biological molecules: a combined Raman, SERS and TERS study. J. Raman Spectrosc. 43 (2012) 1895−1904.

[47] N. Biswas, A. J. Waring, F. J. Walther, R. A. Dluhy, Structure and conformation of the disulfide bond in dimeric lung surfactant peptides SP-$B_{1–25}$ and SP-$B_{8–25}$. Biochim. Biophys. Acta 1768 (2007) 1070–1082.

[48] E. López-Tobar, B. Hernández, M. Ghomi, S. Sanchez-Cortes, Stability of the disulfide bond in cystine adsorbed on silver and gold nanoparticles as evidenced by SERS data. J. Phys. Chem. C 117 (2013) 1531−1537.

[49] J.-E. Clément, A. Leray, A. Bouhelier, E. Finot, Spectral pointillism of enhanced Raman scattering for accessing structural and conformational information on single protein. Phys. Chem. Chem. Phys. 19 (2017) 458−466.

[50] G. Diaz Fleming, J. J. Finnerty, M. Campos-Vallette, F. Célis, A. E. Aliaga, C. Fredesa, R. Koch, Experimental and theoretical Raman and surface-enhanced Raman scattering study of cysteine. J. Raman Spectrosc. 40 (2009) 632–638.

[51] B. Sjöberg, S. Foley, B. Cardey, M.Enescu, An experimental and theoretical study of the amino acid side chain Raman bands in proteins. Spectrochim. Acta A 128 (2014) 300–311.

[52] A. Rygula, K. Majzner, K. M. Marzec, A. Kaczor, M. Pilarczyka, M. Baranska, Raman spectroscopy of proteins: a review. J. Raman Spectrosc. 44 (2013) 1061−1076.

[53] F. Wei, D. Zhang, N. J. Halas, J. D. Hartgerink, Aromatic amino acids providing characteristic motifs in the raman and SERS spectroscopy of peptides. J. Phys. Chem. B 112 (2008) 9158–9164.

[54] S. Reymond-Laruinaz, L. Saviot, V. Potin, M. C. Marco de Lucas, Protein–nanoparticle interaction in bioconjugated silver nanoparticles: A transmission electron microscopy and surface enhanced Raman spectroscopy study. Appl. Surf. Sci. 389 (2016) 17–24.

[55] C. Garrido, T. Aguayo, E. Clavijo, J. S. Gómez-Jeria, M. M. Campos-Vallette, The effect of the pH on the interaction of L-arginine with colloidal silver nanoparticles. A Raman and SERS study. J. Raman Spectrosc. 44 (2013) 1105–1110.

[56] B. Hernández, Y.-M. Coïc, F. Pflüger, S. G. Kruglik, M. Ghomi, All characteristic Raman markers of tyrosine and tyrosinate originate from phenol ring fundamental vibrations. J. Raman Spectrosc. 47 (2016) 210–220.

[57] Z. Chi, X. G. Chen, J. S. W. Holtz, S. A. Asher, UV resonance Raman-selective amide vibrational enhancement: quantitative methodology for determining protein secondary structure. Biochemistry 37 (1998) 2854−2864.

[58] S. Bonnin, F. Besson, M. Gelhausen, S. Chierici, B. Roux, A FTIR spectroscopy evidence of the interactions between wheat germ agglutinin and N-acetylglucosamine residues. FEBS Letters 456 (1999) 361−364.

[59] D. E. Schlamadinger, J. E. Gable, J. E. Kim, Hydrogen bonding and solvent polarity markers in the UV resonance Raman spectrum of tryptophan: application to membrane proteins. J. Phys. Chem. B 113 (2009) 14769–14778.

[60] P. Sevilla, S. Sánchez-Cortés, J. V. García-Ramos and A. Feis, Concentration-controlled formation of myoglobin/gold nanosphere aggregates, J. Phys. Chem. B 118 (2014) 5082−5092.

[61] D. Zhang, O. Neumann, H. Wang, V. M. Yuwono, A. Barhoumi, M. Perham, J. D. Hartgerink, P. Wittung-Stafshede and N. J. Halas. Gold nanoparticles can induce the formation of protein-based aggregates at physiological pH, Nano Lett. 9 (2009) 666−671.

[62] J. M. Zook, V. Rastogi, R. I. MacCuspie, A. M. Keene and J. Fagan, Measuring Agglomerate Size Distribution and Dependence of Localized Surface Plasmon Resonance Absorbance on Gold Nanoparticle Agglomerate Size Using Analytical Ultracentrifugation, ACS Nano 5 (2011) 8070–8079.

[63] C. Schubert Wright and N. Raikhel, Sequence variability in three wheat germ agglutinin isolectins: products of multiple genes in polyploid wheat, J. Mol. Evol. 28 (1989) 327–336.

[64] I. García, J. Mosquera, J. Plou and L. M. Liz-Marzán, Plasmonic Detection of Carbohydrate-Mediated Biological Events, Adv. Optical Mater. 6 (2018) 1800680.

Supplementary Material

Micrographs of AuNPc and AuNPtg films. SERS spectrum of AuNPtg functionalized at intermediate concentration. Extended Raman spectrum of solid WGA.

Acknowledgment

Financial support from the University of Florence (fund RICATEN 2017) is acknowledged.

Figures

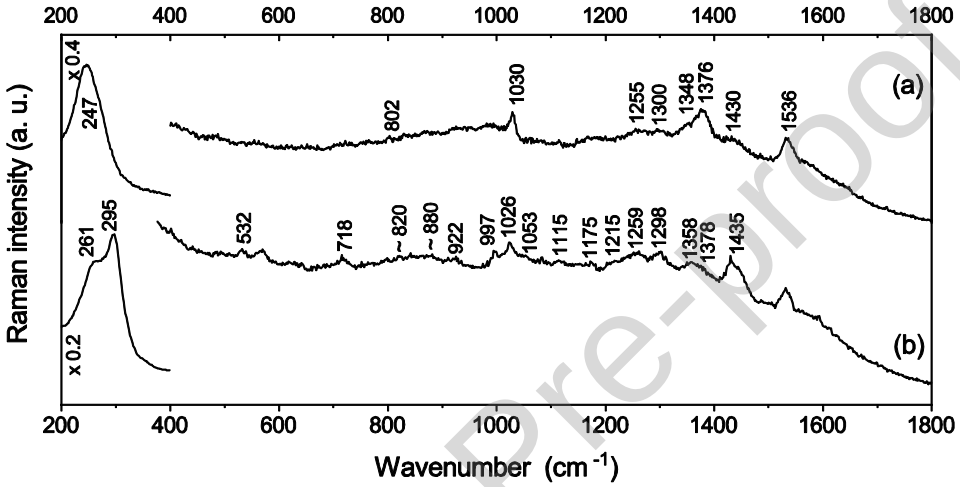

Figure 1

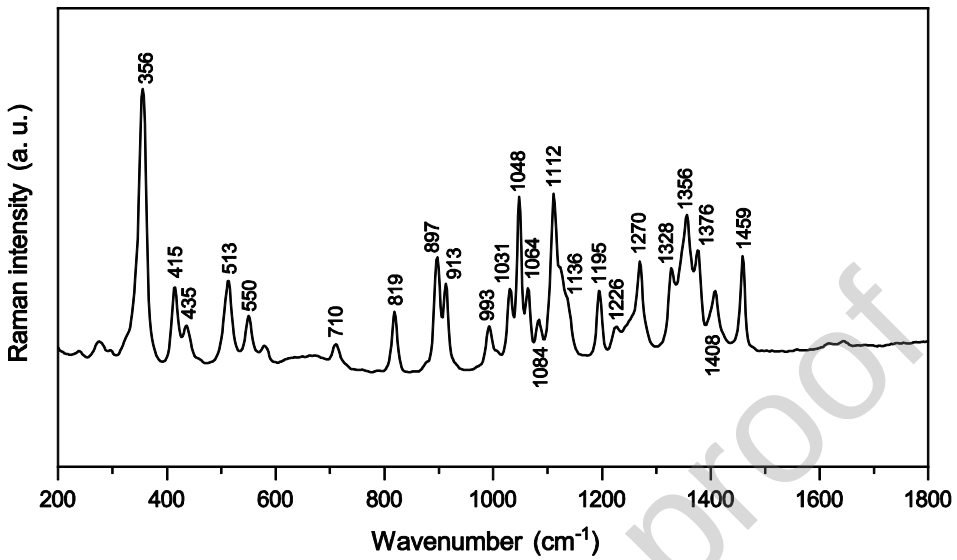

Figure 2

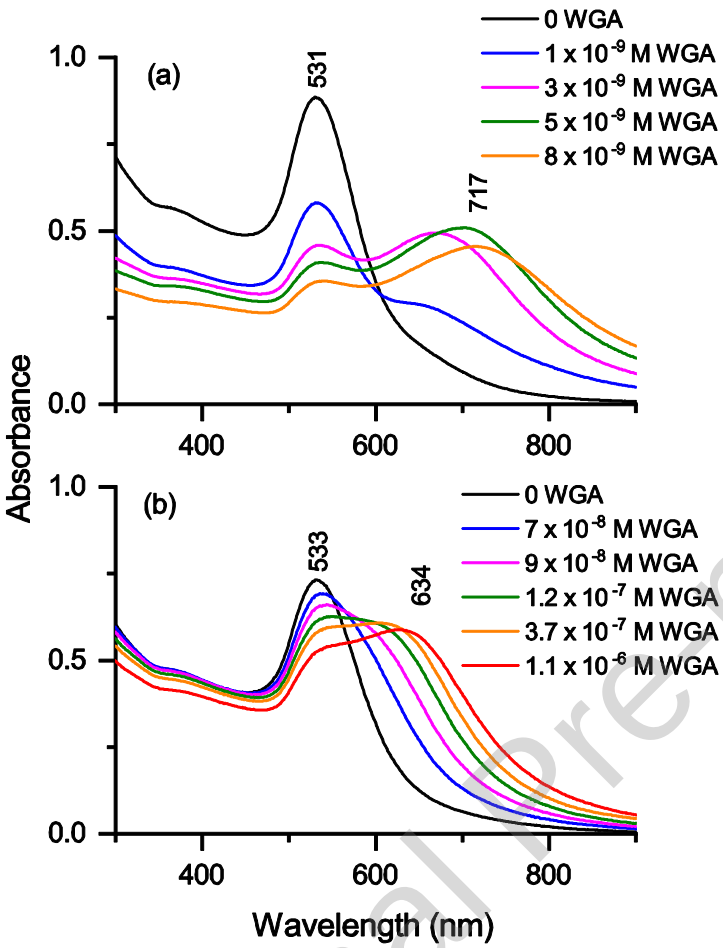

Figure 3

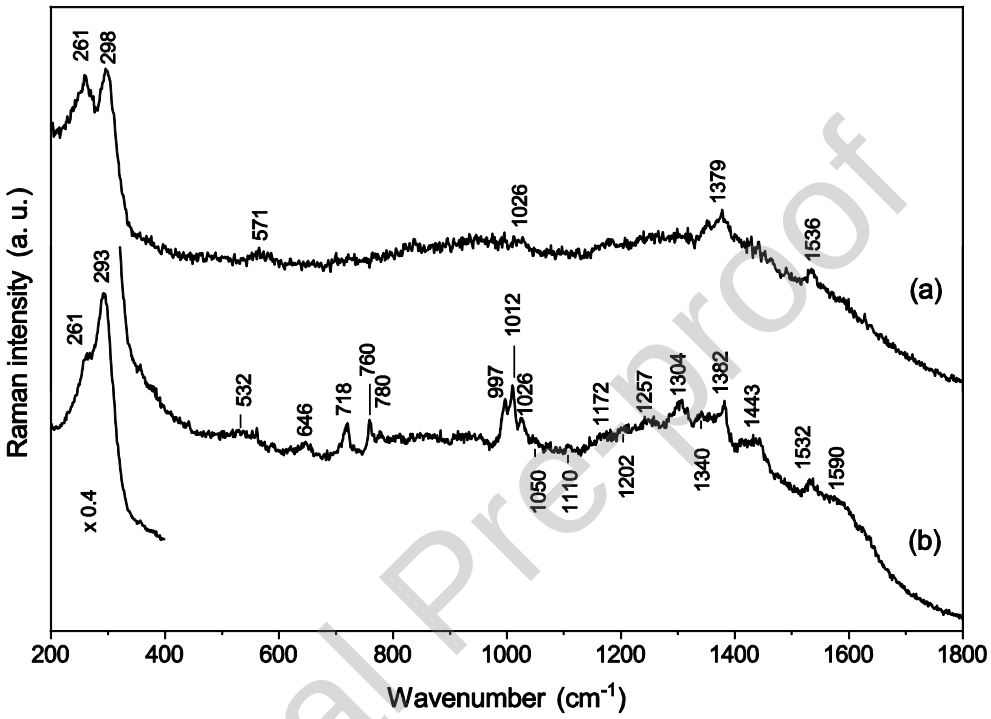

Figure 4

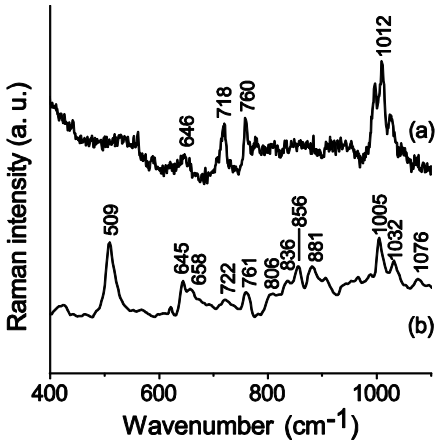

Figure 5